1996A&A...312..256B

Astron. Astrophys. 312, 256–262 (1996)

ASTRONOMY AND ASTROPHYSICS

The dust/gas correlation at high Galactic latitude

F. Boulanger[1], A. Abergel[1], J.-P. Bernard[1], W.B. Burton[2], F.-X. Désert[1], Dap Hartmann[2,3], G. Lagache[1], and J.-L. Puget[1]

[1] Institut d'Astrophysique Spatiale, Bât. 121, Université Paris XI, F-91405 Orsay Cedex, France
[2] Sterrewacht Leiden, Postbus 9513, 2300 RA Leiden, The Netherlands
[3] Harvard-Smithsonian Center for Astrophysics, 60 Garden St., Cambridge, MA 02138, USA

Received 13 March 1995 / Accepted 22 March 1996

Abstract. We have correlated the far-infrared emission from dust as measured by the DIRBE and FIRAS experiments with the 21-cm emission from gas as measured by the Leiden/Dwingeloo survey of HI in our Galaxy. A tight correlation is observed at high $|b|$ at wavelengths ranging from 100 μm to 1 mm. The dust emission spectrum derived from the correlation is fit well by a single Planck curve characterized by T = 17.5 K and an emissivity proportional to ν^2. The dust emissivity τ/N_H = 1.0 $10^{-25}(\lambda/250\,\mu\mathrm{m})^{-2} cm^2$ is remarkably close to the value in the Draine and Lee (1984) dust model and is much smaller than values predicted for porous or fractal grains. In the emission from HI gas, we exclude the presence of a very cold dust component with comparable emissivity, unless its temperature is significantly smaller than 7 K. We also discuss the contribution from Galactic molecular and ionized gas to the global IR emission.

Key words: ISM: atoms – ISM: dust, extinction – ISM: molecules – ISM: general – infrared: interstellar: continuum

1. Introduction

By providing the first maps of the diffuse infrared emission at high Galactic latitudes, the Infrared Astronomical Satellite (IRAS) opened new perspectives on interstellar matter. The IRAS observations were used to probe the spatial distribution of dust, to study its emission properties in different environments, and to investigate the nature of the association of interstellar dust and gas. A decade later, two instruments on board the Cosmic Background Explorer (COBE), namely the Diffuse Infrared Background Experiment (DIRBE) and the Far-Infrared Absolute Spectrophotometer (FIRAS), allow these studies to be extended to the entire emission spectrum of dust ranging from near-infrared to millimeter wavelengths.

Wright et al. (1991) used FIRAS data to derive the first emission spectrum of dust complete beyond 100 μm. They concluded that the spectrum may not be fit with a single dust temperature and therefore proposed the existence of a very cold dust component with a temperature of about 6 K. More recently Reach et al. (1995) pursued this line of analysis by presenting the results of a two-component fit as a function of Galactic coordinates. Here, we analyze the FIRAS and DIRBE far-infrared data from a different perspective by correlating the distribution of the IR emission at high $|b|$ with that of the interstellar gas, following the analysis method applied by Boulanger & Pérault (1988) to IRAS data and older HI material. We focus on the high-$|b|$ sky because there it is relatively straightforward to identify and separate the contribution of the different gas components to the IR emission. The sky at high $|b|$ is, furthermore, largely transparent to HI emission, just as it is to infrared emission from dust, so that gas/dust correlations will be largely free of saturation effects. We highlight here results concerning the spectral and spatial properties of the interstellar emission on large angular scales. A particular motivation of this work was to improve understanding of Galactic emission in regions of low gas column density in order to support the search for an extragalactic infrared background presented in a companion letter (Puget et al. 1996).

Send offprint requests to: F. Boulanger

2. IR and HI data sets

The COBE data used here are those released to the community at the end of 1994. The DIRBE experiment mapped the sky with 40′ resolution in 10 spectral bands at wavelengths ranging from 1.25 to 240 μm (see Silverberg et al. 1993). We restrict this analysis to the DIRBE maps at the longer wavelengths, namely at 100, 140, and 240 μm. To facilitate the removal of zodiacal-light contamination we used only those maps made with data interpolated at a solar elongation of 90° (see DIRBE Explanatory Supplement). FIRAS is a Michelson interferometer which provided coverage, at an angular resolution of 7°, of emission in the complete spectral range from 2.2 to 96 cm^{-1} (4.5 mm to 104 μm), with a fixed spectral resolution of 0.57 cm^{-1} (see Fixsen et al. 1994 and other COBE publications for technical details and calibration procedures). The FIRAS spectrometer, has two independent detectors operated in two scanning modes lead-

© European Southern Observatory • Provided by the NASA Astrophysics Data System

1996A&A...312..256B

ing to four independent sets of sky maps. We use here only the so-called RHSS and LLSS maps because these provide the best signal-to-noise characteristics for both the high ($\lambda < 500\,\mu$m) and low frequency ($\lambda > 500\,\mu$m) ranges.

The HI data used here is that of the new Leiden/Dwingeloo survey, which covers the entire sky North of $\delta = -30°$ with a grid spacing of 0.°5 in both l and b. The 36′ HPBW of the Dwingeloo 25-m telescope provides 21-cm maps at an angular resolution which closely matches that of the DIRBE maps. The kinematic coverage of the material spans velocities in the range $-450 < v_{\rm LSR} < +400$ km s^{-1} at a spectral resolution of 1.03 km s^{-1}. The spectra have been corrected for contamination from stray radiation to a characteristic rms level on the measured brightness temperatures of 0.07 K. The data of the Leiden/Dwingeloo survey represent an improvement over earlier large-scale surveys by an order of magnitude or more in at least one of the principal parameters of sensitivity, spatial coverage, or spectral resolution. Details of the observational and correction procedures are given by Hartmann (1994) and by Hartmann & Burton (1995). The correction for stray radiation is of particular importance to the analysis reported here, because in regions of low total HI column densities, up to 50% of the emission in the uncorrected spectra is contributed by stray radiation entering the sidelobes of the antenna.

The first step in the data analysis is to prepare maps of the IR Galactic emission from the COBE data sets. To do so, we had to subtract the contributions from the Cosmic Microwave Background and the zodiacal emission. For the Cosmic Mircrowave Background we used the well determined parameters (including those describing the dipole structure) given by Reach et al. (1995). The subtraction of the zodiacal light is formally a much more difficult problem but at long wavelengths ($\lambda > 100\,\mu$m) a simple model provides a sufficiently accurate subtraction. The large difference between Galactic and zodiacal emission spectra allows using the 25-μm DIRBE map as a template for the zodiacal light. At high $|b|$, Galactic emission in the $25\mu m$ map, after scaling to $100\mu m$ by the zodiacal emission ratio, amounts to less than 1% of the $100\mu m$ emission. This fraction is significantly higher only near isolated star-forming regions; such regions are rare at high $|b|$, and, in any case, the gas/dust correlation in these regions is not relevant here. Bright, point-like sources were removed from the $25\mu m$ DIRBE map using a median filter at constant ecliptic latitude. The resulting template was scaled to the longer wavelengths by a constant factor for the entire map. This is a simplification since the zodiacal emission spectrum does depend on the ecliptic latitude but Galactic maps derived from this assumption show no clear evidence of zodiacal residuals even at $100\mu m$. The mean ratio between the zodiacal emission at 100 μm and at 25 μm was estimated as 0.16; longward of 100 μm, we followed Reach et al. (1995) in using an emission spectrum decreasing as ν^3. At ecliptic latitudes $|\beta| > 30°$, the spatial variation of the zodiacal emission is fit well by a cosecant law. In order to normalize the zero level of the zodiacal emission we assumed that the emission at the ecliptic pole is equal to the slope of the $csc(\beta)$ variation. This holds if around the poles the zodiacal cloud geometry may be locally approximated by a plane parallel disk. None of the results presented in this paper depend on this assumption.

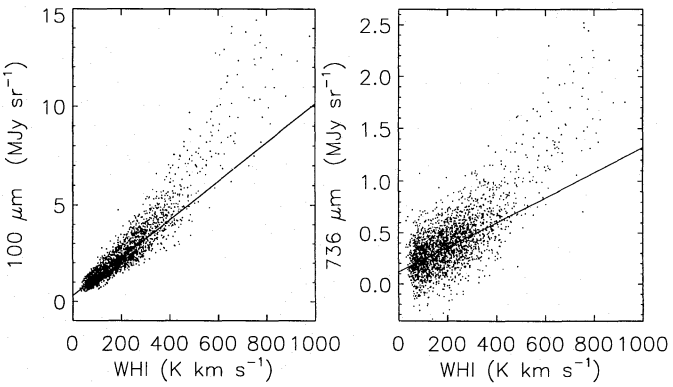

Fig. 1. Correlation between IR and HI emission at 100 μm (DIRBE data, smoothed to 7° resolution) and at 736 μm (FIRAS LLSS data, averaged between 600 and 900 μm). The lines represent fits to data at $W_{\rm HI} < 250$ K km s^{-1}. Above this threshold, the correlation persists but with a higher IR/HI emission ratio (see Sect. 5.1).

Table 1. Infrared/HI dust-to-gas correlation

$\lambda(\mu$m)	S (Slope)	I (Intercept)
DIRBE resolution		
100	0.53 ± 0.00	0.31
140	1.26 ± 0.01	0.88
240	1.07 ± 0.01	0.86
FIRAS resolution		
100D	0.54 ± 0.01	0.30
140D	1.28 ± 0.02	0.81
240D	1.08 ± 0.01	0.72
346	0.53 ± 0.01	0.60
490	0.23 ± 0.03	0.23
535	0.17 ± 0.01	0.29
736	0.065 ± 0.004	0.14
1100	0.016 ± 0.003	0.05

Note:
Definition of parameters: IR (MJy/sr)= $S \times N_{\rm HI}/10^{20}$ HI cm^{-2} + I

For comparison with the DIRBE data we projected the HI data onto the sky using the COBE projection algorithm. For comparisons with the FIRAS data, we first smoothed both the DIRBE and the HI maps to the FIRAS resolution of 7°. The FIRAS sky cubes were averaged in wavelength bins to produce broad-band photometric maps centered at λ = 346 and 490 μm, for the RHSS data, and at 535, 736, and 1100 μm, for the LLSS data. We also produced FIRAS maps convolved with the 140- and 240-μm DIRBE filters. The fluxes were color-corrected for the Galactic spectrum derived in Sect. 4.

3. IR/HI dust-to-gas correlation

Aspects of the dust-to-gas relationships among HI column densities, Lick Galaxy counts and reddening of galactic and extragalactic objets were analyzed by Burstein and Heiles (1978).

© European Southern Observatory • Provided by the NASA Astrophysics Data System

1996A&A...312..256B

Their work raised important astrophysical questions which could not be verified with the data then at hand. A zero point offset was found in the relation between reddening and HI column density and the dust-to-gas ratio was found to vary widely from region to region. Note that the Burstein and Heiles work was based on Hat Creek HI data so restricted in velocity that in many directions most of the gas emission was ignored. The launch of the IRAS satellite opened a new perspective on this topic. Several studies based on the IRAS data showed that the 100-μm emission away from $b \sim 0°$ and away from the principal nearby molecular complexes is generally tightly correlated with the distribution of the neutral atomic gas (e.g. Boulanger & Pérault 1988; Deul and Burton 1993). Some of these studies have focussed on regions where the dust component is correlated with HI emission which lies at velocities outside the coverage of the first HI high latitude surveys (Deul and Burton 1990).

Here we pursue the dust-to-gas correlation analysis exploiting the wavelength coverage and sensitivity of the DIRBE and FIRAS missions on the one hand, and the sensitivity and velocity coverage of the Leiden/Dwingeloo HI material on the other. A significant correlation is observed between IR and HI emission at all wavelengths from 100 μm to 1 mm (Fig. 1). $W_{\rm HI}$ was determined over the velocity range $v_{\rm LSR} \leq 100$ km s^{-1}. This range includes the regime of intermediate-velocity clouds which not uncommonly have a dust counterpart (Deul & Burton 1990), as well as most of the signature of the warped HI outer-Galaxy layer which may extend to latitudes as high as 45°; the high-velocity-cloud objects lie outside this range, but they have no detectable dust emission at the level of the low velocity gas (Wakker & Boulanger 1986). The IR-HI correlation is tight for $W_{\rm HI} < 250$Kkms^{-1}; for higher $W_{\rm HI}$ the data points depart from the the low emission correlation and the scatter is much larger (Fig. 1). The excess IR emission at the higher $W_{\rm HI}$ values was also noted in the correlation diagrams made by Deul & Burton (1993; see their fig. 35) using IRAS 100-μm data; they interpreted the changing slope in terms of a non-neglible optical depth of the HI line at some directions through the Galactic gas layer. In Sect. 5.1 we argue that the break in the correlation is due to emission from dust associated with molecular gas. Here, we restrict the analysis to the lower $W_{\rm HI}$ values and to higher $|b|$ where the assumption of HI optical thinness and low H_2 abundance seems justified. The IR-HI emission ratios listed in Table 1 were derived from a least-squares fit to data points with an HI column depth, $W_{\rm HI}$, less than 250 K km s^{-1} (for optically thin emission 1 K km s^{-1} = 1.82 10^{18} cm^{-2}). Note that the 100μm value listed in Table 1 is significantly smaller than that derived from a similar analysis witht the IRAS data, 0.85 MJy/sr for 10^{20}Hcm^{-2}. This is related to the known calibration difference between DIRBE and IRAS.

In the linear regressions the HI material served as the independent variable because of its high signal-to-noise characteristics. However, if the IR emissivity of the HII gas is comparable to that of HI the relevant variable would be the total gas column density. In this case, using the N(HI) alone to represent the total dust column density introduces an error in the independent variable which we have ignored. The effect of the contribution from HII gas on the IR-HI correlation results depends of course on the actual IR emissivity of HII gas (see Sect 5.2) but also on the degree of spatial correlation between the neutral and ionized gas. If the HII and HI are spatially correlated, the IR/HI emission ratios may be overestimated by as much as 30% (the mean HII/HI column density ratio at high latitude) because the correlation analysis normalizes the IR emission of both the HI and HII gas by only the HI column density. In the limit were the HII and HI are completley uncorrelated, N(HII) may be considered as a stochastic error on the independent variable, N(HI), used for fitting. Then the least square fit that minimizes the error in the IR emission will give an IR/HI emission ratio smaller than the true correlation ratio. This effect has been discussed by Wright (1992) with respect to correlation studies between diffuse UV light and HI column density.

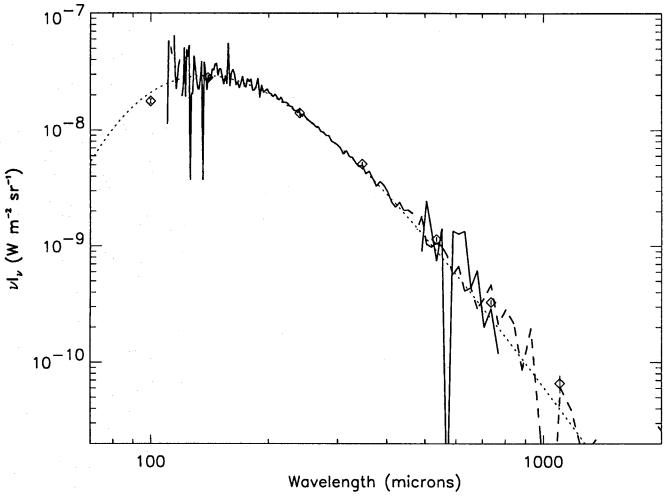

Fig. 2. Far-infrared spectrum of interstellar dust associated with HI gas, normalized for 10^{20} H cm^{-2}. In addition to continuum emission from dust, the 158-μm line of C^+ is seen. The high (RHSS) and low (LLSS) parts of the spectrum are shown by full-drawn and dashed lines, respectively; a few spectral points at $\lambda > 500\mu m$ are much noiser than their neighbors (see Fixsen et al. 1994). The dust emission is fit by a Planck curve with an emissivity index of 2 and a temperature of 17.5 K (dotted line). The diamonds represent the csc(b) slopes of Table 2, scaled by 0.85.

4. Dust emission spectrum

To compute the emission spectrum from dust associated with HI gas, we extracted from the HI map (smoothed to the FIRAS resolution) all pixels with $W_{\rm HI} < 250$ K km s^{-1} (representing about 36% of the sky). We divided these pixels into two groups of roughly equal size, according to whether $W_{\rm HI} < 140$ K km s^{-1} or $140 < W_{\rm HI} < 250$ K km s^{-1}. The Fig. 2 emission spectrum is the difference between the two mean spectra computed from these two sets of points; forming the difference effectively removes any residual dust emission not correlated with the HI. The difference spectrum has been normalized per unit HI column density by dividing it by the difference in mean HI emission.

© European Southern Observatory • Provided by the NASA Astrophysics Data System

1996A&A...312..256B

The FIRAS spectrum is fit well by a single modified Planck curve with emissivity $\tau/N_H = 1.0\ 10^{-25}(\lambda/250\,\mu\mathrm{m})^{-2} cm^2$ and a temperature of 17.5 ± 0.2K. The uncertainty on τ comes essentially from the unknown contribution of dust in the diffuse ionized gas (See Sect. 3 and 5.2). The τ value given here may be overestimated by as much as 30% (the mean HII/HI fraction at high latitude) if the HI and HII gas are tightly correlated. The temperature is in the range of values measured by Sodroski et al. (1994) from the 140 and 240μm DIRBE data, for the Galactic plane emission outside of the molecular ring.

The ν^2 emissivity law corresponds to what is expected for compact dielectric grains. The graphite and silicate grains in the Draine & Lee (1984) model also have a far-IR emissivity varying as ν^2. The τ value derived from the FIRAS data is remarkably close to the value of $1.1\ 10^{-25} cm^2$ at 250μm for this model while the far-infrared emissivities computed for porous and fractal grains are higher by at least a factor of a few (Wright 1987, Mathis & Whiffen 1989, Bazell & Dwek 1990). The FIRAS spectrum thus suggests that grains in the diffuse interstellar medium are compact rather than porous. Mathis & Lee (1991) reached a similar conclusion for dust in the Galactic plane, based on a study of X-ray scattering by dust. Neininger et al. (1996) have recently estimated the mm optical depth of dust associated with HI gas in outer parts of the spiral galaxy NGC 4565. Their value is also in very close agreement with the Draine and Lee value. The value given by Pajot et al. (1989) for the diffuse emission in the direction of the molecular ring is a factor 2 higher.

Draine and Anderson (1985) computed the dust emission spectrum for the Draine and Lee model and the local interstellar radiation field. The equilibrium temperatures of graphite and silicate grains, 18.8 and 15.4 K for a 0.1μm grain, are signifcantly different from the FIRAS temperature. This spectrum is thus signifcantly warmer than the FIRAS spectrum; it is fit well by a single temperature, 18.2 ± 0.2K and a ν^2 emissivity law although it includes emission of grains at a range of temperature. This example shows that the spread in temperature over the size distribution and the contribution from silicates produce a widening of the far-IR spectrum which is small and difficult to identify (see Appendices in Mathis et al. 1983). The FIRAS temperature must thus be considered as a mean temperature averaged over the size distribution and possibly various types of grains.

The residuals to the one-temperature fit of the FIRAS spectrum are shown in Fig. 3. Outside a few noisy data points they are close to zero for $\lambda > 250\mu m$. Over these wavelengths the residuals show no hint for an additional, very cold, component at the level found by Reach et al. (1995). Assuming a temperature of 7 K for this purported component we can set an upper limit on the optical depth ratio $\tau(7\,\mathrm{K})/\tau(17.5\,\mathrm{K}) \sim 1$ (the lower dotted curve in Fig. 3); this contrasts with the ratio of 7 found at high $|b|$ by Reach et al. A very cold component with significant emissivity is clearly not present in the dust correlated with emission from HI gas unless its temperature is significantly smaller than 7 K. For $\lambda < 250\mu m$ the residuals clearly depart from zero but the difference is still small in proportion to the full emission (the upper dotted curve in Fig. 3 corresponds to 1/10 of the 17.5 K fit of Fig. 2). The FIRAS residuals are positive down to $\lambda = 200\mu m$. At shorter wavelengths the FIRAS data is too noisy but we compared the 17.5 K spectrum with the DIRBE 100 and 140μm infrared to HI emission ratio listed in Table 1. The 17.5 K spectrum is 8% higher at 140μm and 30% at 100μm. To better account for the emission spectrum around its peak it is probably necessary to introduce a small spread in grains temperatures and a flattening of the emissivity law for $\lambda < 250\mu m$ relative to the long-wavelengths ν^2 dependendence.

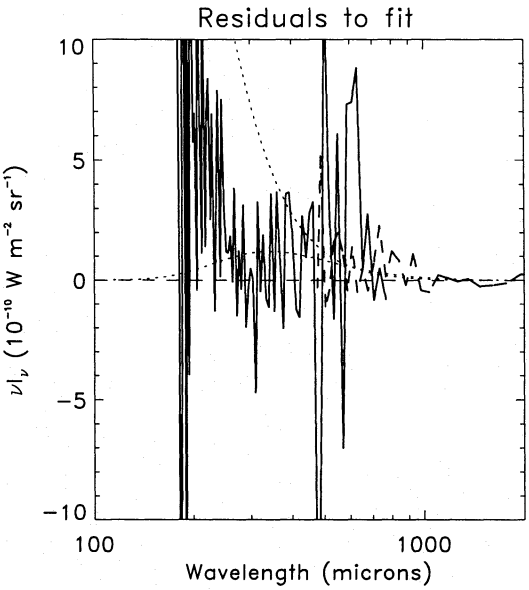

Fig. 3. Difference spectrum between the H I emission spectrum and the 17.5 K fit shown in Fig. 2. The high (RHSS) and low (LLSS) parts of the spectrum are shown by full-drawn and dashed lines, respectively; a few spectral points at $\lambda > 500\mu m$ are much noiser than their neighbors (see Fixsen et al. 1994). Two dotted curves are shown. The lower one corresponds to a Planck curve for a temperature of 7 K and an emissivity equal to that of the 17.5 K component in Fig. 2. The upper dotted curve is 1/10 of the 17.5 K spectrum in Fig. 2.

To check the possibility that a very cold Galactic component does exist but is uncorrelated with the HI gas we measured the spectrum of the Galactic emission by computing latitude profiles at the set of wavelengths for which we have built broad-band photometric maps from the FIRAS data (Sect. 2). The latitude profiles were computed by averaging data within bins at fixed steps in csc(b). Data in the direction of the Magellanic Clouds and towards the principal nearby molecular clouds Orion, Ophiucus, Taurus, and Perseus were not used; few pixels with a bright infrared excess were also discarded. The profiles have been fitted by cosecant laws; the slopes of the cosecant fits computed for $|b| > 20°$ are given in Table 2. In the second column, the normalization per gas column density was done by dividing the cosecant slopes by the slope of the HI cosecant law computed for the same data points, 176 K km/s or $3.2 10^{20}$Hcm^{-2} for optically thin emission. The cosecant slopes measure the overall emission from all Galactic disk components while the normalization done in the Table considers only the H I gas. In Fig. 2 the

© European Southern Observatory • Provided by the NASA Astrophysics Data System

1996A&A...312..256B

Table 2. Slopes of cosecant fits

$\lambda(\mu m)$ μm	MJy/sr	normalized to HI MJy/sr for $N_{HI} = 10^{20}$ Hcm^{-2}	residual MJy/sr
100 D	2.20 ± 0.09	0.69 ± 0.03	0.35 ± 0.04
140 D	4.26 ± 0.17	1.33 ± 0.05	0.20 ± 0.09
240 D	4.45 ± 0.20	1.39 ± 0.06	0.06 ± 0.08
240 F	4.18 ± 0.22	1.31 ± 0.07	0.38 ± 0.12
346	2.19 ± 0.09	0.68 ± 0.03	0.22 ± 0.07
490	0.94 ± 0.04	0.29 ± 0.01	0.08 ± 0.10
535	0.76 ± 0.03	0.24 ± 0.01	0.13 ± 0.05
736	0.30 ± 0.01	0.094 ± 0.003	0.035 ± 0.011
1100	0.09 ± 0.01	0.03 ± 0.003	0.027 ± 0.016

Note: D and F in the first column correspond to DIRBE and FIRAS data, respectively. The residuals tabulated in column 4 refer to values fitted over the range of longitudes given in the text (Sect. 5.2) after subtraction of the HI contribution to the IR emission .

slopes of the cosecant fits are compared with the HI spectrum. The plotted values have been scaled by a factor 0.85 to adjust the $240\mu m$ cosecant point with the HI spectrum. This scaling factor empirically accounts for the fact that we ignored the molecular and ionized gas in the normalization of the cosecant slopes per hydrogen atom or ion. The cosecant points approximately follow the HI emission spectrum. The slight departure observed at the two longest wavelengths deserves further investigation but the good agreement observed at $536\mu m$ and shorter wavelengths shows that near the solar neighborhood there is no cold emission component of importance significant on large angular scales. Puget et al. (1996) show that the cold component found at high $|b|$ by Reach et al. (1995) does not show any variation with Galactic longitude and latitude nor ecliptic latitude. They interpret this isotropic residual as due to distant galaxies. The results presented here do not exclude that localized features may have flatter emission spectra (like that near $b = 0°$, see Wright et al. 1991) because of localized changes in dust properties and/or because of the characteristics of the localized radiation environment. Balloon observations of individual regions on degree scales in the dust sub-mm continuum also led Fischer et al. (1995) to report an emission spectrum flatter than a ν^2 single-temperature spectrum.

The spectrum in Fig. 2 also shows the C^+ emission line at 158 μm. This detection implies a C^+ emission of $3.0 \pm 0.4\ 10^{-26}$ ergs s^{-1} per H atom, a value in agreement with estimates from absorption-line studies by Morris et al. (1991) and by Gry et al. (1992) as well as with the far-IR measurements by Bock et al. (1993). The line-to-continuum ratio, $I(C^+)/\nu I_\nu(158\ \mu m) \sim 0.009 \pm 0.0015$, agrees well with the mean Galactic-plane value of 0.0082 reported by Wright et al. (1991). The signal to noise of the FIRAS data is unsufficient to detect the NII line emission expected from the high $|b|$ diffuse HII gas.

5. Contribution from molecular and ionized gas to the dust/gas correlation

We investigated the residuals of the IR/HI correlation for evidence of molecular and ionized gas which might have a dust counterpart contributing to the overall IR sky emission. The 100-μm residual map made using full-resolution DIRBE data shows numerous features readily identifiable with known molecular clouds, isolated regions of heated dust, and intermediate-velocity clouds (Boulanger et al. 1995); here, we focus on the global, rather than local, properties of the residuals.

5.1. Molecular gas

The data in the Fig. 1 IR/HI correlations depart from the low-W_{HI} correlation line for $W_{HI} > 300$ K km s^{-1}; the same trend is observed in the higher-resolution DIRBE data. Deul and Burton (1993) interpreted the changing slope, which they already noticed with IRAS data, by a non-negligible optical depth of the HI line. This interpretation cannot be ruled out without further investigation but we favor here the idea that the break is related to the contribution of molecular gas to the IR emission. The only direct information about the abundance of molecular hydrogen in the Solar Neighborhood comes from Copernicus measurements of H_2 absorption lines in the spectra of stars. Based on spectra obtained with that satellite, Savage et al. (1977) pointed out that the fraction of molecular gas shows a sudden increase to values ~ 0.1 for a color excess $E(B-V) \sim 0.08$ which corresponds to $N_{HI} = 5\ 10^{20}$ H cm^{-2}. Above this threshold, the median value of the molecular-gas fraction is observed to increase with N_{HI}. This result has been interpreted as the effect of self-shielding on the abundance of H_2. The fact that the break in the IR-HI correlation coincides with the column density threshold found with the Copernicus data is unlikely to be a mere coincidence. It strongly suggests that the change in slope in the IR-HI correlation is associated with an increasing contribution of molecular gas for N_{HI} larger than the threshold value. This interpretation is also supported by the tendency for most of the corresponding data points to cluster on the sky within and around well-known molecular complexes (see map in Boulanger et al. 1995).

5.2. Diffuse ionized gas

Another gas component which might be detectable in the dust/gas correlation maps is the diffuse H^+ gas. Observations of H_α emission at high $|b|$ and of dispersion measures in the direction of pulsars at high $|z|$ indicate that low-density ionized gas (the Warm Ionized Medium, WIM) accounts for some 25% of the gas in the solar neighborhood, with a vertical column density measured from the mid-plane in the range $0.8 - 1.4\ 10^{20}$ H cm^{-2} (Reynolds 1989). The scale height of this gas component is estimated to be 1.5 kpc. The WIM is the dominant component of the interstellar medium at $|z| > 1kpc$. Since most of the grain destruction is expected to occur in the low density components of the interstellar medium (McKee 1989), the WIM could well be dust poor. The search for dust emission from the WIM is

© European Southern Observatory • Provided by the NASA Astrophysics Data System

1996A&A...312..256B

important to understand the evolution of dust in low density gas and through the acceleration processes required for carrying gas far-away from the Galactic mid-plane.

The IR emission from any dust associated with the WIM would follow a csc(b) variation, like that from any diffuse component in the Galactic disk. Boulanger & Pérault (1988) searched unsuccessfully in the 100-μm IRAS all-sky map for such a contribution. This is a difficult problem because one cannot easily separate the contribution of the HII gas from that of HI gas. Little information about the spatial distribution of the WIM is available and the little information we have shows that part of the WIM is spatially correlated with HI gas (Reynolds et al. 1995). Kogut et al. (1996) have also shown that the free-free emission from the WIM is correlated with the far-IR emission from dust on large angular scales ($> 7°$). Consequently part of the IR emission associated with the WIM is removed from the data when we subtract the contribution from the HI gas. We simulated the effect of IR emission from the WIM on the IR-HI correlation analysis in the following way. We assumed that the WIM has an IR emissivity per hydrogen ion equal to that of the HI gas and that it is distributed in the sky like the 240μm sky emission at the same Galactic longitude but opposite latitude. This last assumption is arbitrary but it ensures that the assumed spatial distribution shares the morphological features of galactic interstellar matter including the dependence with Galactic latitude. After proper normalization we added this simulated contribution to that of the HI directly scaled from the HI map using the fit to the spectrum of Fig. 2. Gaussian noise was added to this data with the same dependence on wavelength than in the real FIRAS data sets. We then processed this simulated data in the same way we processed the real data. The IR-HI emission spectrum we derived from this simulation was exactly proportional to the spectrum we had put in with a scaling factor of 1.18. This simulation can of course only be illustrative but it shows that even without a direct association between HI and HII gas, IR emission from the HII gas can lead to a significant overestimate of the IR emission from the HI gas. In this case the 18% bias represents about half of the contribution of the WIM we had put in the simulation. For the purpose of this paper it is important to stress that this bias does not affect the shape of the spectrum.

In the companion paper (Puget et al. 1996), the FIRAS data in regions of low HI emission was used to extrapolate the IR-HI correlation to zero H I emission. We processed the simulation data in the same way and found a non-zero emission at zero HI emission with a spectrum exactly proportional to the input spectrum for the HI emission. This emission results from the fact that the linear extrapolation to zero HI column density does not fully remove the IR emission associated with the HII gas. Here, the simulation illustrates what is discussed by Puget et al.: the infrared emission for zero-HI emission computed with the FIRAS data may be partly explained by Galactic emission uncorrelated with HI gas but not fully because the spectrum is very different from the Galactic spectrum found for the HI gas.

If present in the data the contribution from the WIM to the IR sky emission is thus partly removed when subtracting the HI component. Part of it, however, is probably left in the residuals and we looked for it by searching a diffuse component in the residuals of the IR-HI correlation with an intensity scaling with $csc(|b|)$. The best part of the sky to look for this emission is the region selected for the computation of the HI emission spectrum in Sect. 4 because there is there little confusion with emission from molecular gas. But the latitude profiles computed with pixels with $W_{\rm HI} < 250$ K km s^{-1} show no measurable gradient with Galactic latitude. Using data with higher HI emissivity allows us to include more points in the analysis, especially at the lower $|b|$ where the Galactic gradient is expected to be strongest. In this case the possibility of confusion with emission from dust associated with molecular gas is real. To minimize this problem we selected two extensive regions where the DIRBE dust/gas residual map shows little structure ($30° < l < 115°$ and $180° < l < 270°$, for $b > 20°$). We fit the latitude profiles computed over these regions with cosecant variations. The measured slopes are given in Table 2. The slopes found for the residual emission are consistent with an emission spectrum like that of the HI gas for $N_{\rm HI} \sim 3 - 5\ 10^{19}$ H cm^{-2}. (Only the 140 and 240 μm DIRBE points would give a much lower value, namely $\sim\ 10^{19}$ Hcm^{-2}; we can not explain this discrepancy.) The column density of $3 - 5\ 10^{19}$ H cm^{-2} is roughly half of the Reynolds's estimate for the total H^+ column density. We consider this as an upper limit for the contribution of the H^+ component left in the data, because the csc(b) slopes could in fact be measuring large-scale variations in the IR/HI emission ratio and/or emission from low contrast molecular clouds. Taking into account that only half of the WIM emission may well be left in the residuals of the IR-HI correlation, this upper limit is still consistent with a normal dust abundance in the WIM.

6. Summary

We have studied the dust-to-gas correlation at high Galactic latitude exploiting both the wavelength coverage and sensitivity of the DIRBE and FIRAS data and the sensitivity and velocity coverage of the Leiden/Dwingeloo HI survey. The main results of this study are the following.

(1) A good correlation is observed between IR and HI emission at all wavelengths from 100μm 1mm for HI column densities smaller than 5 10^{20}Hcm^{-2}. For higher HI column densities there is a change in the correlation slope and the scatter is much larger. This break in the correlation occurs for a column density equal to the threshold value where Copernicus observations show that the fraction of molecular gas becomes significant. We thus argue that it is the infrared emission from molecular gas which affects the IR-HI correlation.

(2) The correlation between infrared and HI emission is used to derive the far-IR and submillimeter spectrum of dust associated with HI gas. This spectrum is fit well by a single Planck curve characterized by T =17.5 K and with an emissivity proportional to ν^2. We show that there is no colder component of importance significant on large angular scales. The dust emissivity $\tau/N_H = 1.0\ 10^{-25}(\lambda/250\,\mu{\rm m})^{-2} cm^2$ is remarkably close

© European Southern Observatory • Provided by the NASA Astrophysics Data System

1996A&A...312..256B

to the value in the Draine and Lee (1984) dust model and is much smaller than values predicted for porous or fractal grains.

(3) We have looked for infrared emission from dust associated with diffuse HII gas at high Galactic latitudes. It is likely that this emission, if it exists, is partly included in the IR-HI correlation. We set an upper limit on what may be left in the residuals of the IR-HI correlation which is still consistent with a normal dust abundance in the warm ionized medium.

Acknowledgements. We are grateful to the Goddard Space Flight Center team for introducing us to the COBE data.

References

Bazell, D. and Dwek, E. 1990, ApJ 360, 142
Bock, J., et al. 1993, ApJ 410, L115
Boulanger, F., Pérault, M. 1988, ApJ 330, 964
Boulanger, F., et al. 1995, in "Unveiling the Cosmic Infrared Background" ed. E. Dwek, (AIP Conf. Proc.)
Burstein, D., Heiles, C. 1978, ApJ 225, 40
Deul, E.R., Burton, W.B. 1990, A&A 230, 153
Deul, E.R., Burton, W.B. 1993, in *The Galactic Interstellar Medium*, (D. Pfenniger & P. Bartholdi, eds.), Springer-Verlag, Heidelberg, p. 79
Draine, B.T. and Lee, H.M. 1984, ApJ 285, 89
Draine, B.T. and Anderson, N. 1985, ApJ 292, 494
Fischer, M.L., et al. 1995, ApJ 444, 226
Fixsen, D.J., et al. 1994, ApJ 420, 457
Gry, C., Lequeux, J., Boulanger, F. 1992, A&A 266, 457
Hartmann, D. 1994, Ph.D. Thesis, University of Leiden
Hartmann, D., Burton, W.B. 1995, Atlas of Galactic HI Emission. Cambridge University Press (under contract)
Kogut, A., Banday, A.J., Bennet, C.L., Górski, K.M., Hinshaw, G., and Reach, W.T. 1996, ApJ in press
McKee, C.F. 1989, in Interstellar Dust, eds. L.J. Allamandola and A.G.G.M. Tielens, p. 431, Kluwer
Mathis, J.S., Mezger, P.G. and Panagia, N. 1983, A&A 128, 212
Mathis, J.S. and Whiffen G. 1989, ApJ 341, 808
Mathis, J.S. and Lee, C.W. 1991, ApJ 376, 490
Morris, S.L., Weymann, R.J., Savage, B.D., Gilliland, R.L. 1991, ApJ 377, L21
Neininger, N., Guélin, M. Garcia-Burillo S., Zylka, R. and Wielebinski, R. 1996, A&A in press
Pajot, F. et al. 1989, A&A 223, 107
Puget, J.L., et al. 1996, A&A 308, L5
Reach, W.T., et al. 1995, ApJ 451, 188
Reynolds, R.J. 1989, ApJ 339, L29
Reynolds, R.J., Tufte, S.L., Kung, D.T., Mc Cullough, P.R., Heiles, C. 1995, ApJ 448, 715
Savage, B.D., Bohlin, R.C., Drake, J.F., Budich, W. 1977, ApJ 216, 291
Silverberg, R.F., et al. 1993, in SPIE Conference Proc. 2019 on Infrared Spaceborne Remote Sensing, San Diego
Sodroski, T.J. et al. 1994, ApJ 428, 638
Wakker, B.P., Boulanger, F. 1986, A&A 170, 84
Wright, E. L. 1987, ApJ 320, 818
Wright, E. L., et al. 1991, ApJ 381, 200
Wright, E. L. 1992, ApJ 391, 34

This article was processed by the author using Springer-Verlag LaTeX A&A style file *L-AA* version 3.

© European Southern Observatory • Provided by the NASA Astrophysics Data System